Space-time correlations of fluctuating velocities in turbulent shear flows

Xin Zhao[1] and Guo-Wei He[1,2,*]

[1]*LNM, Institute of Mechanics, Chinese Academy of Sciences, Beijing 100080, People's Republic of China*
[2]*Department of Aerospace Engineering, Iowa State University, Ames, Iowa 50011-2271, USA*
(Received 9 August 2008; published 16 April 2009)

Space-time correlations or Eulerian two-point two-time correlations of fluctuating velocities are analytically and numerically investigated in turbulent shear flows. An elliptic model for the space-time correlations in the inertial range is developed from the similarity assumptions on the isocorrelation contours: they share a uniform preference direction and a constant aspect ratio. The similarity assumptions are justified using the Kolmogorov similarity hypotheses and verified using the direct numerical simulation (DNS) of turbulent channel flows. The model relates the space-time correlations to the space correlations via the convection and sweeping characteristic velocities. The analytical expressions for the convection and sweeping velocities are derived from the Navier-Stokes equations for homogeneous turbulent shear flows, where the convection velocity is represented by the mean velocity and the sweeping velocity is the sum of the random sweeping velocity and the shear-induced velocity. This suggests that unlike Taylor's model where the convection velocity is dominating and Kraichnan and Tennekes' model where the random sweeping velocity is dominating, the decorrelation time scales of the space-time correlations in turbulent shear flows are determined by the convection velocity, the random sweeping velocity, and the shear-induced velocity. This model predicts a universal form of the space-time correlations with the two characteristic velocities. The DNS of turbulent channel flows supports the prediction: the correlation functions exhibit a fair good collapse, when plotted against the normalized space and time separations defined by the elliptic model.

I. INTRODUCTION

An important concept in the turbulence theory is that small-scale eddies are progressively decorrelated in time. The decorrelation process can be characterized by two-time two-point correlations of fluctuating velocities, or simply, space-time correlations. The space-time correlations are fundamental to the turbulence theory and have a broad application. The classic direct interaction approximation (DIA) theory [1] and various Eulerian closure theories [2–4] need a model for space-time correlations to derive energy spectra. In isotropic turbulence, a space-time-correlation model is developed from the random sweeping hypothesis and then used to formulate the universal scaling of the energy spectra [2]. However, in turbulent shear flows, such a space-time-correlation model is not available, which obstructs the derivation of the energy spectra. In the recently developed mapping closure approximation for probability density functions [5,6] and the functional derivative closure for scalar mixing [7], a space-time-correlation model is also needed. In many applications such as aeroacoustics [8,9], the frequency spectra of sound are calculated from the space-time correlations. The recent application of large eddy simulation (LES) to sound prediction in turbulent flows requires the correct prediction of LES on the space-time correlations [10]. In isotropic turbulence, the space-time correlations are mainly determined by instantaneous energy spectra. Consequently, an accurate prediction of LES on energy spectra implies the accurate prediction of LES on the space-time correlations

[11]. However, in turbulent shear flows, the space-time correlations may not be determined by the energy spectra at resolved scales. A further understanding of space-time correlations could help the developments of LES in predicting turbulent noise.

The decorrelation process of small eddies with time can arise either by the sweeping of small eddies by energy-containing eddies or the distortions of small eddies themselves. In homogeneous and isotropic turbulence, the decorrelation process of small eddies is dominated by the energy-containing eddies [12,13]. Therefore, the decorrelation time scales of space-time correlations are mainly determined by the sweeping velocity defined as the rms of fluctuating velocities [14]. However, in turbulent shear flows, the large-scale shear flows induce the distortions of small eddies while the latter is carried downstream. Generally, it is difficult to discriminate between those two effects. The well-known Taylor frozen flow hypothesis [15] suggests that the small eddies are carried past a fixed point by the mean flows without any essential change. It implies that the space-time correlations are determined by a convection velocity. However, Taylor's model has many limitations such as a weak shear rate and low turbulence intensity [16,17]. Based on the Kovasznay [18] and Corrsin's conjecture [19], Farve proposed that the space-time correlations can be expressed in terms of the space correlations and its probabilistic diminution with time. The *ad hoc* choice of the probabilistic diminution is crucial to the success of the model [20].

Our previous rapid communication [21] empirically proposed an elliptic model for space-time correlations in turbulent shear flows. It is a second approximation to the isocorrelation contours while Taylor's model is a first approximation to the contours. The purpose of this paper is to rationally develop the elliptic model for the space and

*Authors to whom correspondence should be addressed; hgw@lnm.imech.ac.cn; guoweihe@yahoo.com

time separations in the inertial range, including a complete derivation of the elliptic model from the similarity hypothesis on isocorrelation contours, the analytical calculations of those two parameters in the model, and a comprehensive numerical verification of the model using the direct numerical simulation (DNS) of turbulent channel flows. The contour similarity assumption can be justified from the well-known Kolmogorov similarity hypotheses. The elliptic model relates the space-time correlations to space correlations via two parameters: the convection and sweeping velocities. We will use the quasinormality assumption to formulate the analytical expressions of the convection and sweeping velocities in homogeneous turbulent shear flows. The expressions clearly indicate the role of mean shear rates. Those results will be used to explore the mechanism of the decorrelation process in turbulent shear flows. The elliptic model will be numerically verified using the DNS date of turbulent channel flows.

The rest of the paper is organized as follows. In Sec. II, we will give a complete derivation of the elliptic model. In Sec. III, we will derive from the Navier-Stokes equation the expressions for the two parameters in the elliptic model: the convection and sweeping velocities. The numerical verification from the DNS of turbulent channel flows will be presented in Sec. IV. Finally, conclusions and discussions will be made in Sec. V.

II. ELLIPTIC MODEL FOR SPACE-TIME CORRELATIONS

The classic space-time-correlation theory in turbulence [12,13] suggests that the dominant effects on space-time patterns at high frequencies is the sweeping of small eddies that pass an observation point by large-scale eddies. This implies that the space-time fluctuations can be expressed as an appropriate transformation of space correlations. The Taylor frozen flow hypothesis is the simplest version of the transformation. To understand this problem, we introduce the Navier-Stokes equations for the turbulent flows

$$\frac{\partial v_i}{\partial t} + v_j \frac{\partial v_i}{\partial x_j} = -\frac{\partial p}{\partial x_i} + \nu \frac{\partial^2 v_i}{\partial x_j \partial x_j},$$

$$\frac{\partial v_i}{\partial x_i} = 0, \tag{1}$$

where $\mathbf{v} = (v_1, v_2, v_3)$, p and ν are the velocity vector and the pressure and the kinematic viscosity, respectively. The repeated indices imply a summation. The velocity field can be decomposed into the mean flow part and the fluctuating part

$$U_i = \langle v_i \rangle, \quad v_i = U_i + u_i, \quad p = \langle p \rangle + p', \tag{2}$$

where the bracket $\langle \ \rangle$ denotes the ensemble averaging. It follows from Eq. (1) that the fluctuating velocity and pressure satisfy

$$\frac{\partial u_i}{\partial t} = -(U_j + u_j)\frac{\partial u_i}{\partial x_j} - u_j \frac{\partial U_i}{\partial x_j} + \frac{\partial \langle u_i u_j \rangle}{\partial x_j} - \frac{\partial p'}{\partial x_i} + \nu \frac{\partial^2 u_i}{\partial x_j \partial x_j},$$

$$\frac{\partial U_i}{\partial x_i} = \frac{\partial u_i}{\partial x_i} = 0. \tag{3}$$

In this paper, we confine the mean velocity field to a simple mean shear flow. $U_1 = U(x_2)$ is only dependent on the normal distance and U_2 and U_3 are negligibly small. The space-time-correlation function is defined as

$$R(r, \tau) = \langle u_i(\mathbf{x}, t) u_i(\mathbf{x} + r\mathbf{e}_1, t + \tau) \rangle, \tag{4}$$

where u_1 is the stream-wise component of a velocity vector (u_1, u_2, u_3), $\mathbf{e}_1$ is the unit vector along the stream-wise direction, $\mathbf{r}$ is a spatial separation vector with r being its magnitude, and τ is a time separation. Taylor's hypothesis assumes that the transformation is linear, such as

$$R(r, \tau) = R(r - U\tau, 0). \tag{5}$$

The linear transformation implies that the isocorrelation contours are straight lines: $r - Ut = C$, where C denotes a contour level (see Fig. 1). Thus, the space-time correlations remain constant for sufficiently large separations r or τ in the linear contours. This result violates the basic property of correlation functions, which decay with increasing separations in either space or time. Therefore, Taylor's model is not correct for larger separations. However, we learn from Taylor's model that the isocorrelation contours is a useful approach to relate space-time correlations to space correlations. The problem with Taylor's model is that a linear approximation is not accurate. Therefore, we should introduce a higher-order approximation to the contours.

We will summarize our previous derivations [21] for the elliptic model as follows. Consider a contour $R(r, \tau) = C$ near the origin $(r, \tau) = (0, 0)$. We expand the correlation function $R(r, \tau)$ in a Taylor power series at the origin up to second order

$$R(r, \tau) = R(0, 0) + \frac{\partial^2 R(0, 0)}{\partial r \, \partial \tau} r\tau$$
$$+ 0.5 \left[\frac{\partial^2 R(0, 0)}{\partial r^2} r^2 + \frac{\partial^2 R(0, 0)}{\partial \tau^2} \tau^2 \right], \tag{6}$$

where $\partial R(0, 0)/\partial r = 0$ due to homogeneity and $\partial R(0, 0)/\partial \tau = 0$ due to stationary. The contour $R(r, \tau) = C$ intersects with the space separation axis at the point $(0, r_c)$, such that

$$R(r, \tau) = R(r_c, 0). \tag{7}$$

Replacing the correlation function R in Eq. (7) by Eq. (6), we obtain

$$r_c^2 = (r - U\tau)^2 + V^2 \tau^2, \tag{8}$$

where

$$U = -\frac{\partial^2 R(0, 0)}{\partial r \, \partial \tau} \left[\frac{\partial^2 R(0, 0)}{\partial r^2} \right]^{-1},$$

$$V^2 = \frac{\partial^2 R(0, 0)}{\partial \tau^2} \left[\frac{\partial^2 R(0, 0)}{\partial r^2} \right]^{-1} - U^2. \tag{9}$$

Equation (8) implies that the isocorrelation contours are elliptic (see Fig. 1). Substituting Eq. (8) into Eq. (7) gives the elliptic model

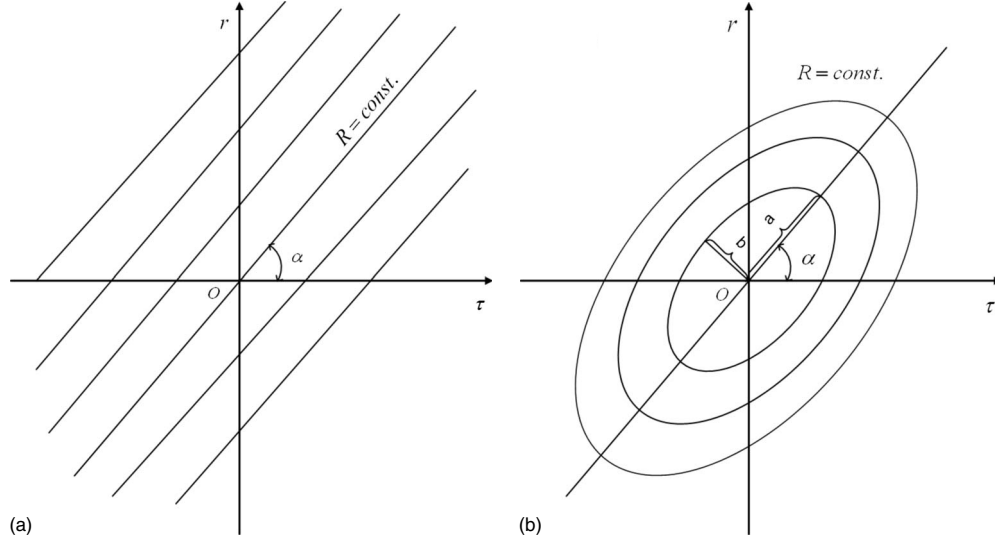$$R(r, \tau) = R[\sqrt{(r - U\tau)^2 + V^2 \tau^2}, 0]. \tag{10}$$

FIG. 1. The schematic diagram for the isocorrelation contours. (a) They are straight lines with a constant slope in Taylor's frozen flow hypothesis; (b) they are elliptic with a uniform preference direction and a constant aspect ratio in the present model.

It is evident that the Taylor expansion is valid for small separations r and τ and thus, the elliptic model is only valid for small separations. The Taylor expansion also generates a good approximation to the space-time correlations at low-Reynolds-number flows, where the second-order terms are dominating [22]. Our previous work suggests that the model is also applicable for larger separations [21]. In this section, we will extend the elliptic model from small separations to the ones in the inertial range. The extension is based on the following two assumptions. (1) The elliptic approximation: the contours of space-time velocity correlations can be essentially approximated by second-order algebraic curves, which are elliptic as shown as in Eq. (8). (2) The contour similarity: at a sufficiently large Reynolds number, the contours of space-time velocity correlations at inertial-range separations share a preference direction and an aspect ratio, where the preference direction is defined as the direction of the major axis in a contour and measured by the slope of the major axis with respect to the horizontal axis, and the aspect ratio is defined as the length ratio of the major axis to the minor one in the contour.

We will postpone the justification of the above two assumptions later in this section and now use them to extend the elliptic model. According to these two assumptions, the isocorrelation contours for large separations are also elliptic and have the same preference direction $\tan \alpha$ and aspect ratio $\lambda \equiv b/a$ as those for small separations

$$\tan^2 \alpha = 4U^2/[\sqrt{(1+U^2-V^2)^2+4U^2V^2}+(1-U^2-V^2)]^2,$$

$$\lambda^2 = 4V^2/[\sqrt{(1+U^2-V^2)^2+4U^2V^2}+(1+U^2+V^2)]^2.$$

$$(11)$$

Therefore, the general form of the isocorrelation contours can be written as

$$(r-U\tau)^2 + V^2\tau^2 = C, \qquad (12)$$

which is the same as Eq. (8) with a contour level C. As a result, we could find the intersecting point $(0, r_c)$ of the contour (12) with the space separation axis, such that $R(r, \tau) = R(r_c, 0)$ holds true for all r and τ on the contour.

The assumption of elliptic approximation can be justified as follows. The isocorrelation contours should be central curves since a space-time correlation has its maximum at origin and decays with increasing separations in space and/or time. A linear approximation to the isocorrelation contours is not accurate as explained before. A second-order approximation to the isocorrelation contours suggests that the contours should be elliptic, since either parabolic or hyperbolic contours imply that the correlation functions do not decay with increasing separations on the contours. The second-order approximation offers the correct estimates of the Taylor microscales and the integral scales via the composition of the isocontour functions into the space correlations. Successively high-order approximation can be achieved, if necessary, by including the higher-order terms of its Taylor-series expansion. However, it does not offer any more essential improvement. Gotoh and Kaneda [23] demonstrated that the results from the second-order approximation to space-time correlations are in agreement with the ones from the Lagrangian renormalized approximation. The elliptic approximation to the isocorrelation contours was used for velocity components in [24,25] and Lagrangian time correlations in [26]. We should note that the elliptic approximations are not accurate for pressure time correlations [27].

Next, we will justify the contour similarity hypothesis (see Fig. 1). The premise for the Kolmogorov similarity hypothesis is taken for granted in this discussion. Every turbulent flow at sufficiently large Reynolds numbers is expected to approach a universal state of scale similarity at small scales [28].

(1) The assumption of a uniform preference direction is developed from the Taylor frozen flow hypothesis. Taylor's

hypothesis implies that the isocorrelation contours have a preference direction. Since the isocorrelation are parallel lines in the frozen flows, the slope of the preference direction is the convection velocity. In the nonfrozen flows, the isocorrelation contours are elliptic rather than straight lines. However, there still exist an effective convection velocity which dominates the motion of small eddies. Therefore, the isocorrelation contours share a preference direction and thus its slope is the convection velocity. The uniform convection velocity has been verified by the theoretical arguments, experimental studies, and numerical simulations [29]. Wills [25] defined the convection velocity as the ratio r_c/τ_c, where r_c maximizes $R(r,\tau)$ for a given τ_c. This definition has been thoroughly investigated and frequently used in many researches [27,30,31]. Kim and Hussian [30] calculated the convection velocity for velocity correlations in turbulent channel flows and the result obtained shows that the ratio varies by less than 0.1 for different τ_c. For more complex, case such as pressure correlations, Choi and Moin [27] pointed out that the uniform convection velocity is a very useful indicator.

(2) The assumption of a constant aspect ratio is derived from the Kolmogorov similarity hypotheses. Since a preference direction does not change the aspect ratio, we simply assume that the preference direction is zero $U=0$. This is the case for isotropic turbulence, which yields

$$R(r,\tau) = R(\sqrt{r^2 + (V\tau)^2}, 0). \tag{13}$$

From the Kolmogorov similarity hypotheses, the velocity structure functions for either space or time separations must have the form [28]

$$D(r,0) = C_K(\epsilon r)^{2/3},$$

$$D(0,\tau) = C_K(\epsilon V\tau)^{2/3}, \tag{14}$$

where C_K is constant and V is a sweeping velocity. Tennekes [13] derived Eq. (14) using the sweeping hypothesis, whose Fourier form gives the well-known scaling of Eulerian time spectra [32]. The velocity structure function is defined by

$$D(r,\tau) = \langle [u_1(\mathbf{x} + \mathbf{r}, t + \tau) - u_1(\mathbf{x}, t)]^2 \rangle. \tag{15}$$

The structure function is related to the space-time correlations via

$$D(r,0) = 2R(0,0) - 2R(r,0), \tag{16}$$

$$D(0,\tau) = 2R(0,0) - 2R(0,\tau). \tag{17}$$

For an elliptic contour $R(r,\tau) = C$, we could find its principal axes lengths τ_c and r_c from $R(0,\tau_c) = R(r_c, 0) = C$. respectively. This implies $D(r_c, 0) = D(0, \tau_c)$. Submission of Eq. (14) into the above equations yields $r_c/\tau_c = V$. Therefore, the aspect ratio is constant.

The elliptic model relates the space-time correlations to the space correlations via two parameters U and V. If V vanishes, the model implies the result from the Taylor frozen flow hypothesis; on the other hand, if U vanishes, the model implies the results from the Kraichnan and Tennekes random

sweeping-velocity hypothesis [12,13]. Therefore, this model provides an integrated treatment on those two extreme cases.

III. CONVECTION AND SWEEPING VELOCITIES IN HOMOGENEOUS SHEAR TURBULENCE

The essential assumption of the elliptic model is the self-similarity of the isocorrelation contours. The contours share a preference direction and an aspect ratio. In terms of Eq. (11), the preference direction and aspect ratio are determined by the convection and sweeping velocities. In this section, we will analytically calculate the convection and sweeping velocities for the homogeneous turbulent shear flow. The analytical calculation is based on the Navier-Stokes equations using the quasinormal assumption. The shear effects are explicitly included into the present calculations up to the second-order time derivatives of fluctuating velocities. The analytical results obtained will be used to study the influences of mean shear rates on the decorrelation processes of fluctuation velocities.

In this section, we confine the following calculations to homogeneous shear flows. The mean velocity **U** has a constant shear rate in the x_1 direction

$$U_i = Sx_2\delta_{i1}, \tag{18}$$

where S is a shear rate and δ_{ij} is a delta function. Therefore,

$$\frac{\partial U_i}{\partial x_j} = S\delta_{i1}\delta_{j2} \equiv A_{ij}. \tag{19}$$

Using this simplification and eliminating the pressure term from Eq. (3), we obtain

$$\frac{\partial u_i}{\partial t} = -U_j\frac{\partial u_i}{\partial x_j} - P_{ijm}(\nabla)(u_ju_m - \langle u_ju_m\rangle) - L_{im}(\nabla)A_{mj}u_j$$
$$+ \nu\frac{\partial^2 u_i}{\partial x_j \partial x_j}, \tag{20}$$

where

$$P_{ijm}(\nabla) = \frac{1}{2}\frac{\partial}{\partial x_m}P_{ij}(\nabla) + \frac{1}{2}\frac{\partial}{\partial x_j}P_{im}(\nabla),$$

$$P_{ij}(\nabla) = \delta_{ij} - \nabla^{-2}\frac{\partial^2}{\partial x_i \partial x_j},$$

$$L_{ij}(\nabla) = \delta_{ij} - 2\frac{\partial}{\partial x_i}\nabla^{-2}\frac{\partial}{\partial x_j}. \tag{21}$$

Recall that the Eulerian space-time correlations are defined as

$$R(r,\tau) = \langle u_i(\mathbf{x}, t)u_i(\mathbf{x} + r\mathbf{e}_1, t + \tau)\rangle. \tag{22}$$

We assume that, at initial time $t=0$, the fluctuating velocity field in Eq. (20) is homogeneous and isotropic with a normal distribution of zero mean. Accordingly, a short-time calculation can be made for the initially homogenous and isotropic velocity field. For small τ and r, we may expand $R(r,\tau)$ in a Taylor power series at $\tau=0$ and $r=0$ up to second order,

$$R(r,\tau) = R(0,0) + R_r r + R_\tau \tau + 0.5[R_{rr}r^2 + 2R_{r\tau}r\tau + R_{\tau\tau}\tau^2],$$
(23)

where

$$R_r \equiv \frac{\partial R(0,0)}{\partial r}, \quad R_\tau \equiv \frac{\partial R(0,0)}{\partial \tau}, \quad R_{rr} \equiv \frac{\partial^2 R(0,0)}{\partial r^2}$$

$$R_{r\tau} \equiv \frac{\partial^2 R(0,0)}{\partial r \, \partial \tau}, \quad R_{\tau\tau} \equiv \frac{\partial^2 R(0,0)}{\partial \tau \, \partial \tau}.$$
(24)

The first two coefficients R_r and R_τ can be easily evaluated from the homogeneity and stationarity assumptions

$$R_r = R_\tau = 0.$$
(25)

The other coefficients R_{rr}, $R_{r\tau}$, and $R_{\tau\tau}$ can be simplified using the integration by parts

$$R_{rr} = \left\langle u_i(\mathbf{x},t)\frac{\partial^2 u_i}{\partial x_1^2}(\mathbf{x},t) \right\rangle = -\left\langle \frac{\partial u_i}{\partial x_1}(\mathbf{x},t)\frac{\partial u_i}{\partial x_1}(\mathbf{x},t) \right\rangle,$$
(26)

$$R_{r\tau} = \left\langle u_i(\mathbf{x},t)\frac{\partial^2 u_i}{\partial x_1 \, \partial t}(\mathbf{x},t) \right\rangle = -\left\langle \frac{\partial u_i}{\partial x_1}(\mathbf{x},t)\frac{\partial u_i}{\partial t}(\mathbf{x},t) \right\rangle,$$
(27)

$$R_{\tau\tau} = \left\langle u_i(\mathbf{x},t)\frac{\partial^2 u_i}{\partial t^2}(\mathbf{x},t) \right\rangle = -\left\langle \frac{\partial u_i}{\partial t}(\mathbf{x},t)\frac{\partial u_i}{\partial t}(\mathbf{x},t) \right\rangle.$$
(28)

The calculation techniques in the following can be found from Refs. [23,33], where the quasinormality is often used.

We will assume that the second-order correlation tensors are isotropic in the following derivation, where no isotropy assumption is made for higher-order statistics. This assumption can be justified as a reasonable approximation. The classic Kolmogorov similarity theory [28] implies that there is an energy cascade process from large scales to small scales, which progressively reduces the effect of mean shear on the small-scale eddies. Therefore, it is postulated that the small-scale statistics of turbulent flows at high Reynolds numbers is universal and isotropy. However, the recent experiment [34] and numerical simulation [35] found that the anisotropy persists even at high Reynolds numbers. For those high but still finite Reynolds numbers, an approximation can be made for small shear numbers [36]. We assume that the time scale τ_S is associated with the mean shear flows, such as $\tau_S \equiv 1/S$, and $\tau_N \equiv (r^2/\epsilon)^{1/3}$ associated with the time scales of the eddies of the length scales r in the inertial range. Thus, the shear number $S_h \equiv \tau_N/\tau_S$ indicates the relative strength of the inertial-scale eddies to the mean shear flows. We expand the spectral correlation function into a series of power S_h

$$Q_{ij}(\mathbf{k},t) \equiv \langle \hat{u}_i(\mathbf{k},t)\hat{u}_j^*(\mathbf{k},t) \rangle = Q_{ij}^{(0)}(\mathbf{k},t) + Q_{ij}^{(1)}(\mathbf{k},t)S_h + \cdots,$$
(29)

where $\hat{u}_i(\mathbf{k},t)$ is the Fourier mode of the fluctuating velocities, and $Q_{ij}^{(0)}(\mathbf{k},t)$ represents the contribution from isotropic part and $Q_{ij}^{(n)}(\mathbf{k},t)$ $(n \geq 1)$ represent the contributions from

anisotropic ones. If the shear number S_h is small, the nonlinear interaction among small-scale eddies is dominating and thus the contribution from the anisotropic parts is ignorable. As a result, the correlation function can be well approximated by the isotropic part. Therefore, in the following calculation, we will use $Q_{ij}^{(0)}(\mathbf{k},t)$ as an approximation to $Q_{ij}(\mathbf{k},t)$ and will not distinguish $Q_{ij}^{(0)}(\mathbf{k},t)$ from $Q_{ij}(\mathbf{k},t)$. Actually, two well-known experiments [34,37] suggest that the second-order statistics in homogeneous turbulent shear flows are isotropic, whereas higher-order statistics are anisotropic.

A. Evaluation of the coefficient R_{rr}

The coefficient R_{rr} can be evaluated from the Fourier modes $\hat{u}_i(\mathbf{k},t)$ of the fluctuating velocities

$$R_{rr} = -\int k_1^2 \langle \hat{u}_i(\mathbf{k},t)\hat{u}_i^*(\mathbf{k},t) \rangle d\mathbf{k}$$

$$= -\frac{1}{3}\int k^2 \langle \hat{u}_i(\mathbf{k},t)\hat{u}_i^*(\mathbf{k},t) \rangle d\mathbf{k} = -\frac{2}{3}\int_0^\infty k^2 E(k) dk,$$
(30)

where the second and third steps invoke the isotropy assumption on the fluctuating velocities and their spectrum tensors,

$$Q_{ij}(\mathbf{k},t) \equiv \langle \hat{u}_i(\mathbf{k},t)\hat{u}_j^*(\mathbf{k},t) \rangle = P_{ij}(\mathbf{k})\frac{E(k)}{4\pi k^2},$$
(31)

$$P_{ij}(\mathbf{k}) = \delta_{ij} - \frac{k_i k_j}{k^2}.$$
(32)

B. Evaluation of the coefficient $R_{r\tau}$

To evaluate the coefficient $R_{r\tau}$, we introduce the Navier-Stokes (20) into Eq. (27). This gives

$$R_{r\tau} = U_j\left\langle \frac{\partial u_i}{\partial x_1}\frac{\partial u_i}{\partial x_j} \right\rangle + \left\langle [L_{im}(\nabla)A_{mj}u_j]\frac{\partial u_i}{\partial x_1} \right\rangle$$

$$+ \left\langle P_{ijm}(u_j u_m - \langle u_j u_m \rangle)\frac{\partial u_i}{\partial x_1} \right\rangle,$$
(33)

where the viscous term is ignored due to a sufficient large Reynolds number. Similarly to the evaluation of the coefficient R_{rr} in Eq. (26), we obtain

$$R_{r\tau} = \frac{2}{3}U_1\int_0^\infty k^2 E(k) dk$$

$$+ + iS\int \left(\delta_{i1} - 2\frac{k_i k_1}{k^2}\right)k_1\langle \hat{u}_2(\mathbf{k})\hat{u}_i^*(\mathbf{k}) \rangle d\mathbf{k}.$$
(34)

The second term in the above equation is equal to zero since the integrand is odd. This yields

$$R_{r\tau} = \frac{2}{3}U_1\int_0^\infty k^2 E(k) dk.$$
(35)

C. Evaluation of the coefficient $R_{\tau\tau}$

The evaluation of the coefficient $R_{\tau\tau}$ is very similar to the ones of the coefficients R_{rr} and $R_{r\tau}$. The difference is that the second-order time derivatives of the velocity fluctuation is needed in the present evaluation. The derivative can be obtained by taking time derivative of the Navier-Stokes (20). These considerations lead to

$$R_{\tau\tau} = -U_j U_k \left\langle \frac{\partial u_i}{\partial x_j} \frac{\partial u_i}{\partial x_k} \right\rangle - \langle (L_{im}(\nabla) A_{mj} u_j)(L_{ik}(\nabla) A_{kl} u_l) \rangle$$

$$- U_k \left\langle \frac{\partial u_i}{\partial x_k} L_{im}(\nabla) A_{mj} u_j \right\rangle - \langle (P_{ijm}(\nabla) u_j u_m)(P_{ikl}(\nabla) u_k u_l) \rangle$$

$$+ \langle P_{ijm}(\nabla) u_j u_m \rangle \langle P_{ikl}(\nabla) u_k u_l \rangle, \tag{36}$$

where

$$U_j U_k \left\langle \frac{\partial u_i}{\partial x_j} \frac{\partial u_i}{\partial x_k} \right\rangle = \frac{2}{3} U_1^2 \int_0^\infty k^2 E(k) dk, \tag{37}$$

$$\langle [L_{im}(\nabla) A_{mj} u_j][L_{ik}(\nabla) A_{kl} u_l] \rangle = \frac{2}{3} S^2 \int_0^\infty E(k) dk, \tag{38}$$

$$U_k \left\langle \frac{\partial u_i}{\partial x_k} L_{im}(\nabla) A_{mj} u_j \right\rangle = 0, \tag{39}$$

$$\langle [P_{ijm}(\nabla) u_j u_m][P_{ikl}(\nabla) u_k u_l] \rangle - \langle P_{ijm}(\nabla) u_j u_m \rangle \langle P_{ikl}(\nabla) u_k u_l \rangle$$

$$= \frac{2}{3} v_0^2 \int_0^\infty k^2 E(k) dk. \tag{40}$$

Here, $v_0^2 = 2 \int_0^{k_e} E(k) dk$ with k_e being the maximum wave number of energetic modes, and thus, it is approximately determined from the kinetic energy. The quantity v_0 is referred to as the random sweeping velocity in Kraichnan's [12] model.

Therefore, we can obtain $R_{\tau\tau}$ from Eqs. (37)–(40)

$$R_{\tau\tau} = -\frac{2}{3} U_1^2 \int_0^\infty k^2 E(k) dk - \frac{2}{3} S^2 \int_0^\infty E(k) dk$$

$$- \frac{2}{3} v_0^2 \int_0^\infty k^2 E(k) dk. \tag{41}$$

Submission of Eqs. (30), (35), and (41) into Eq. (9) yields the expressions for the convection and sweeping velocities

$$U = U_1, \tag{42}$$

$$V^2 = S^2 \lambda_T^2 + v_0^2, \tag{43}$$

where $\lambda_T^2 = \int_0^\infty E(k) dk / \int_0^\infty k^2 E(k) dk$ is the Taylor length microscale.
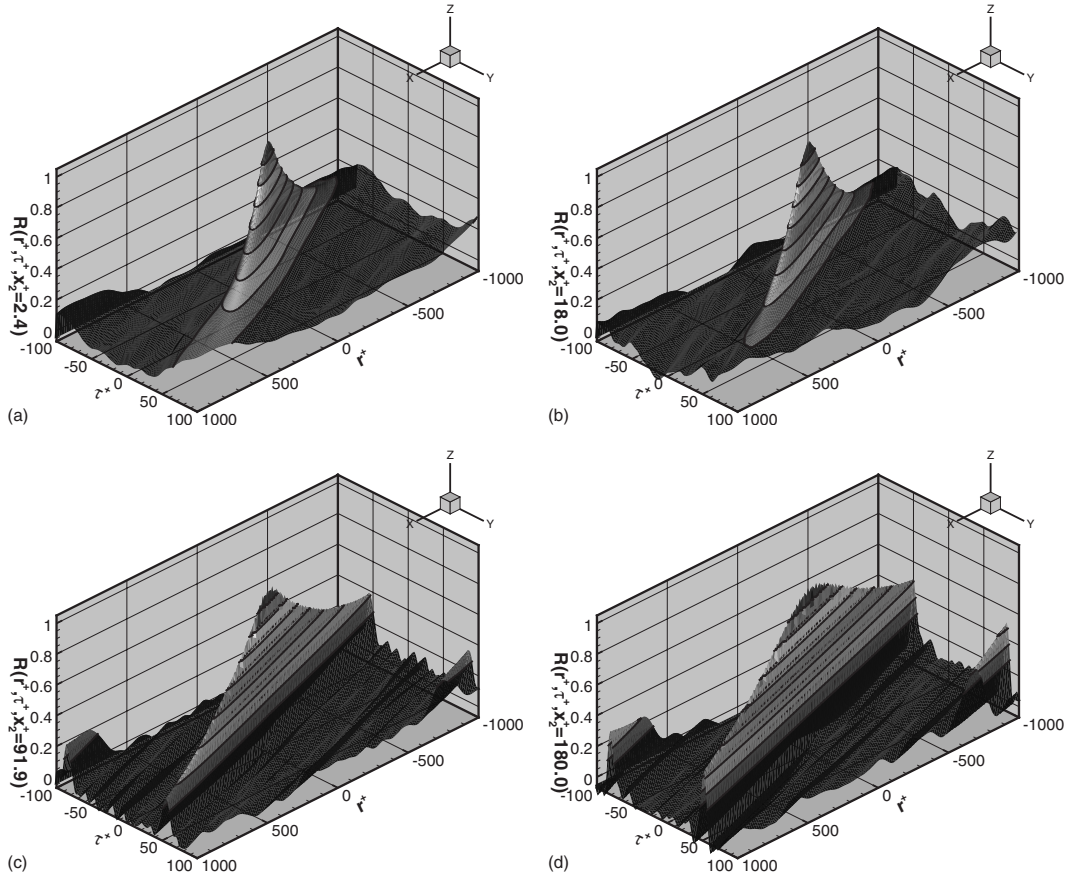

FIG. 2. The surfaces of space-time correlations as functions of space separation and time delay at (a) $x_2^+ = 2.4$ (viscous sublayer), (b) $x_2^+ = 18.0$ (buffer layer), (c) $x_2^+ = 91.9$ (log-law region), and (d) $x_2^+ = 180$ (outer layer). They are approximately fitted by the paraboloidal surfaces suggested by Burghelea *et al.* [38].
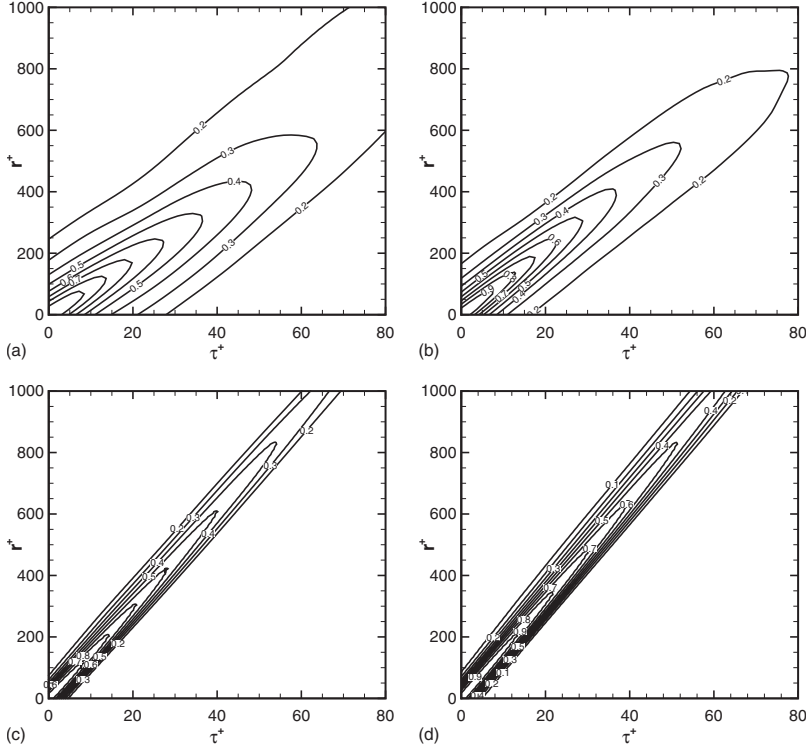
FIG. 3. The contours of space-time correlations as functions of space separation and time delay at (a) $x_2^+ = 2.4$ (viscous sublayer), (b) $x_2^+ = 18.0$ (buffer layer), (c) $x_2^+ = 91.9$ (log-law region), and (d) $x_2^+ = 180$ (outer layer). The contour levels are from 0.2 to 0.9 with increments of 0.1.

It can be seen from Eqs. (42) and (43) that the convection velocity is only determined by the mean velocity and the sweeping velocity determined by the shear rate, the Taylor microscale, and the random sweeping velocity. The latter indicates that shear increases the sweeping velocity and thus decrease the decorrelation time scales of fluctuating velocities. Although the calculations in this section is limited to homogeneous shear flows, the conclusion has a useful implication to inhomogeneous cases. Moreover, if the mean velocity U_1 is dominating but the shear rate and the turbulence intensity are relatively small then the convection velocity U is dominating and the sweeping velocity V could be ignored. In this case, the Taylor frozen flow hypothesis is valid; if the mean velocity is zero, the convection velocity is zero and the sweeping velocity is equal to the random sweeping velocity, which is the case for the Kraichnan and Tennekes sweeping hypothesis. This fact suggests that the present model is a plausible interpolation between those two limits.

IV. NUMERICAL VERIFICATION OF THE ELLIPTIC MODEL IN TURBULENT CHANNEL FLOWS

In this section, we will use the DNS of turbulent channel flows to verify the similarity assumptions and the elliptic model in turbulent shear flows. The similarity assumptions imply that the isocorrelation contours share a uniform preference direction and a constant aspect ratio. We will calculate the preference directions and aspect ratios for each family of icocorrelation contours at the different locations away from the wall, in order to find whether or not they are constant. The elliptic model implies that the space-time correlations are mainly determined by the convection and sweeping velocities. Therefore, the normalized correlation functions

using Eq. (10) should be independent of the convection and sweeping velocities and thus collapse into a universal form. We will examine this prediction using the DNS data.

A direct numerical simulation of fully developed turbulent channel flows has been performed. The incompressible Navier-Stokes and continuity equations were integrated in time using the fractional step method. A modified third-order Runge-Kutta scheme was used for the nonlinear term treated explicitly and second-order Crank-Nicholson scheme was used for the viscous terms treated implicitly. A second-order finite-volume method was used to represent the spatial derivatives. The computation domain was $4\pi\delta$, 2δ, and $2\pi\delta$ in the stream-wise, normal, and spanwise directions, where δ is a length unit. The corresponding grid numbers were $128 \times 129 \times 128$. A nonuniform mesh was used in the wall normal direction. The first mesh point away from the wall was at $x_2^+ = 0.17$ and the maximum spacing at the centerline of the channel was 7.39 wall units. The friction Reynolds number was $\mathrm{Re}_\tau = 180$.

The space-time correlations of fluctuating velocity u_1 in the stream-wise direction is used to verify the elliptic model. The ensemble average is taken as the averaging over the $x_1 x_3$ plane and time t, since the stream-wise component is spatially homogeneous in the $x_1 x_3$ plane and temporally stationary.

Figure 2 plots the surface of the space-time correlations at $x_2^+ = 2.4$ (viscous sublayer), 18.0 (buffer layer), 91.9 (log-law region), and 180.0 (outer layer). The surfaces decay most slowly in the preference directions and most fast in its normal directions. Small oscillations are observed at large separations due to negative correlations. Burghelea *et al.* [38] suggested that the surface can be fitted by a paraboloidal surface for sufficiently small space and time separations.

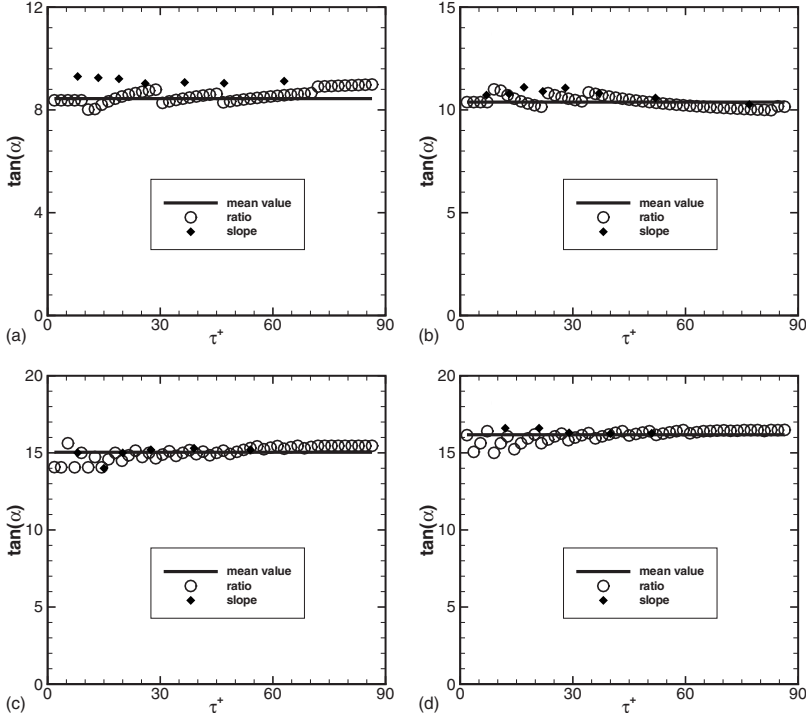Figure 3 displays the isocorrelation contours at $x_2^+ = 2.4$,

FIG. 4. The preference directions of isocorrelation contours as functions of time delays. The circles denote the results from the ratio r_c/τ_c, where r_c maximizes $R(r,\tau)$ for a given τ_c. They are fitted by their mean values (solid lines). The solid diamonds denote the results from the slopes of the major axes of the isocorrelation contours. (a) $x_2^+=2.4$ (viscous sublayer), (b) $x_2^+=18.0$ (buffer layer), (c) $x_2^+=91.9$ (log-law region), and (d) $x_2^+=180$ (outer layer).

18.0, 91.9, and 180.0. It is clearly observed that these curves are approximately elliptic with their preference directions. The slopes of the preference directions become large with increasing x_2^+ from the wall to the centerline. Meanwhile, the elliptic contours become elongated in shape, which indicates that the aspect ratio becomes small. All of those observations are in agreement with the theoretical predictions in Secs. II and III.

Figure 4 shows the preference direction as a function of time separations at the same locations as the ones in Fig. 2. The preference directions are directly calculated from the DNS data $\tan(\alpha)=r^*/\tau^*$, where r^* makes $R(r^*,\tau^*)$ a maximum for each τ^*. They appear to be nearly uniform, which is in agreement with Kim and Hussain's observations in the Appendix of [30]. We further calculate the preference directions using the slopes of the major axes of the isocorrelation contours. They are almost uniform and closed to the ones from the ratios. Hinze [29] pointed out that the two different calculations tend to give the same values for large space separation and convection velocity. Again, it is clearly seen that the preference directions increase with the distance x_2^+ from the wall.

Figure 5 presents the lengths of major axes of the isocorrelation contours as a function of the lengths of their minor axes at the locations $x_2^+=2.4$, 18.0, 91.9, and 180. The lengths of the axes are directly calculated from the DNS data. The length of a major axis is the largest distance between two points on the isocorrelation contours and the length of a minor axis is the smallest distance between them. It is observed that the points are nearly located in a straight line. Moreover, the ratios, which are represented by the slopes of each straight lines, become large with decreasing x_2^+. However, some points on the two ends are deviated from the straight lines. The possible reason for it is that the inertial ranges here are not sufficiently extensive due to the relatively lower Reynolds number in the present simulation.

Figure 6(a) shows the evolution of the space-time correlations with respect to time separations for different space separations $r^+=0$, 84.42, 168.8, 253.3, 337.7, and 422.1 at the location $x_2^+=18.0$. These correlation curves initially increase to the maximum and then decrease. We plot the positive parts of those curves together with the separation axis defined by the convection-velocity-dependent variable $r_T=r-Ut$ in Fig. 6(b) and with the one defined by the convection- and sweeping-velocity-dependent variable $r_E=\sqrt{(r-U\tau)^2+(V\tau)^2}$ in Fig. 6(c). Here, the parameters U and V are directly calculated from the DNS data. Evidently, these curves in Fig. 6(c) collapse very well while the ones in Fig. 6(b) do not collapse especially around the peaks at $r_T=0.0$. This collapse indicates that the second-order Taylor-series expansion yields a better approximation than the first order one even in the viscous layer, where the Reynolds number is relatively lower.

The parameters U and V in Fig. 6(c) are calculated directly from the DNS data. We first calculate the isocorrelation contours using the DNS data and then extract the preference directions $\tan\alpha$ and the aspect ratios λ from the isocorrelation contours. The quantities $\tan\alpha$ and λ are used to calculate the convection velocity U and the sweeping velocity V in terms of Eq. (11). The parameters U and V obtained are averaged so that the averaged convection and sweeping velocities are used in Fig. 6(c). Hereafter, we will call this method as *direct calculation*. The direct calculation gives $U=11.0$ and $V=1.97$. The two parameters can be also obtained by *curve fitting*. We first find the parameter U for $V=0$ such that the peaks of all correlation functions are located at the origin and then adjust the parameter V such that all of them collapse. The curve fitting gives $U=11.5$ and $V=2.23$. These two sets of the parameters are very close and the latter also yields a good collapse [see Fig. 6(d)].
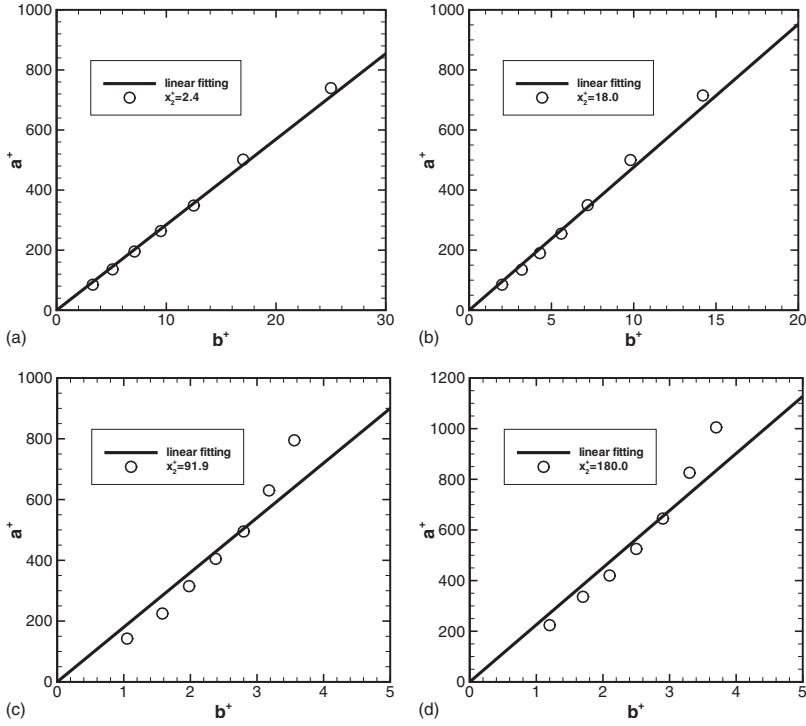
FIG. 5. The aspect ratios of isocorrelation contours as functions of time delays. (a) $x_2^+=2.4$ (viscous sublayer), (b) $x_2^+=18.0$ (buffer layer), (c) $x_2^+=91.9$ (log-law region), and (d) $x_2^+=180$ (outer layer). They are fitted by the straight lines of the slopes equal to the aspect ratio.

We plot the correlation functions for $x_2^+=2.4$ (viscous sublayer) in Fig. 7, $x_2^+=91.9$ (log-law region) in Fig. 8, and $x_2^+=180.0$ (outer region) in Fig. 9, respectively, in the same way as those in Fig. 6. For comparison, Fig. 8(c) is plotted using U and V obtained from the direct calculation and Fig. 8(d) is plotted using U and V obtained from the curve fitting. The two parameters U and V in Fig. 7 are obtained from the direct calculation while the two parameters in Fig. 9 are obtained from the curve fitting, since the preference directions and aspect ratios in Fig. 9 are difficult to be calculated from

the isocorrelation contours. Those figures suggest that the elliptic model is valid for space-time correlations in the inertial range with appropriate parameters U and V.

The convection and sweeping velocities obtained from the theoretical results (42) and (43) and direct calculation using the DNS data are shown in Fig. 10. The direct calculation results are consistent with the previous ones [30]. The theoretical results are the good approximations to the direct calculation ones in the buffer layer, the log-law region, and the outer region. However, both convection and sweeping ve-
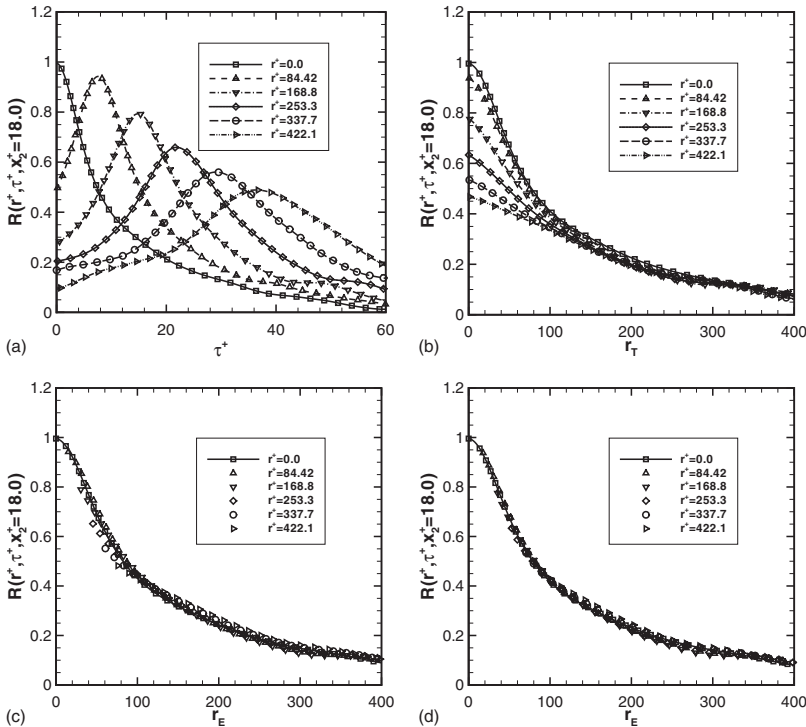

FIG. 6. The space-time correlations R at $x_2^+=18.0$ for different space separation $r^+=0.0$, 84.42, 168.8, 253.3, 337.7, and 422.1 are plotted against (a) time separation, (b) the separation $r_T=r-Ut$ defined from Taylor's frozen flow hypothesis, (c) the separation $r_E=\sqrt{(r-U\tau)^2+(V\tau)^2}$ defined from the elliptic model, with $U=11.0$ and $V=1.97$ obtained from direct calculation, and (d) the same separation as the one in (c) with $U=10.5$ and $V=2.30$ obtained from curve fitting.
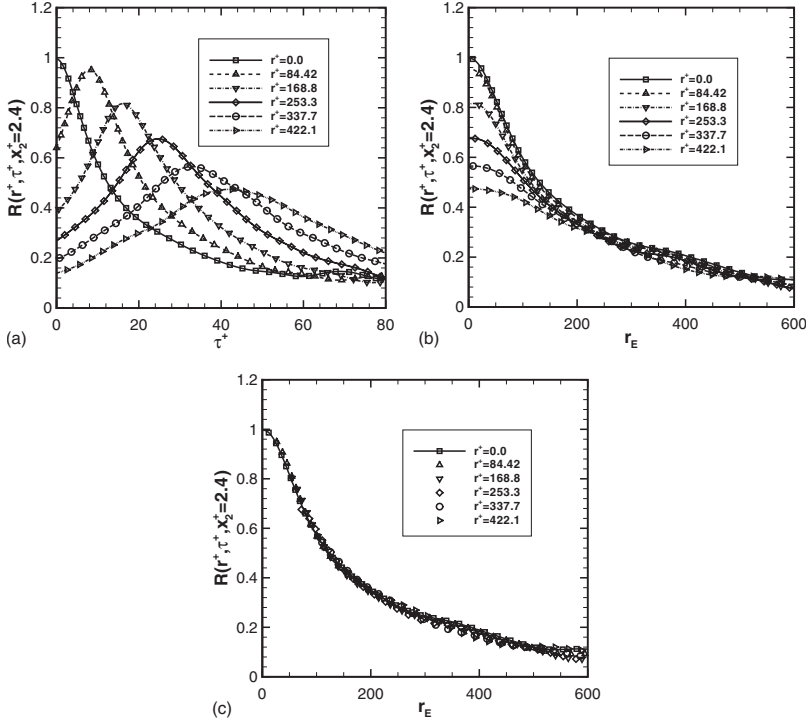
FIG. 7. The space-time correlations R at $x_2^+=2.4$ for different space separations are plotted against (a) time separation, (b) the separation $r_T=r-Ut$ defined from Taylor's frozen flow hypothesis, and (c) the separation $r_E=\sqrt{(r-U\tau)^2+(V\tau)^2}$ defined from the elliptic model, with the parameters U and V obtained from direct calculation.

locities are under predicted in the viscous sublayer, since the shear rates are not small. To closely look at the sweeping velocity, we plot the shear-induced velocity and random sweeping velocity separately in Fig. 10(c), where the mean shear rate, Taylor's microscales, and the random sweeping velocity are evaluated from the DNS data. It is observed that the shear-induced velocity has a peak about $y^+=6$ in the viscous sublayer with a narrow width. The shear-induced velocity makes large contributions to the sweeping velocity in the viscous sublayer with small contributions to the one in other

sublayers. The random sweeping velocity manifests the turbulence intensity.

The elliptic model is verified from the DNS of turbulent channel flows. The collapses of correlation functions using the elliptic model are observed in viscous sublayer, buffer layer, log-law region, and outer region, while the collapses using the Taylor frozen flow hypothesis are only observed in the outer region. The characteristic velocities U and V in the model are obtained from either direct calculation or curve fitting. Both of them yield the satisfactory results.
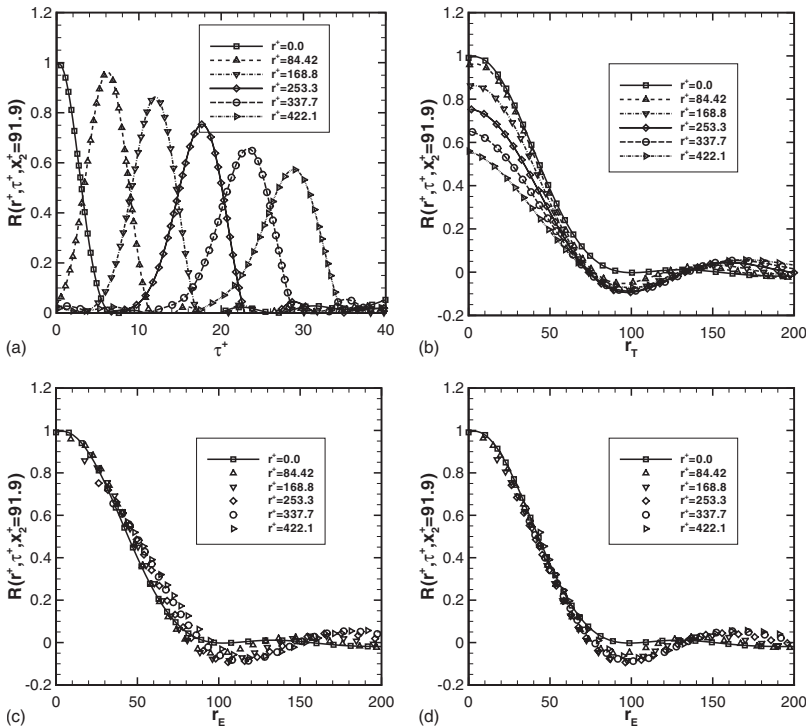

FIG. 8. The space-time correlations R at $x_2^+=91.9$ for different space separations are plotted against (a) time separation, (b) the separation $r_T=r-Ut$ defined from Taylor's frozen flow hypothesis, (c) the separation $r_E=\sqrt{(r-U\tau)^2+(V\tau)^2}$ defined from the elliptic model, with $U=15.1$ and $V=1.41$ obtained from direct calculation, and (d) the same separation as the one in (c) with the parameters $U=14.5$ and $V=1.50$ obtained from curve fitting.

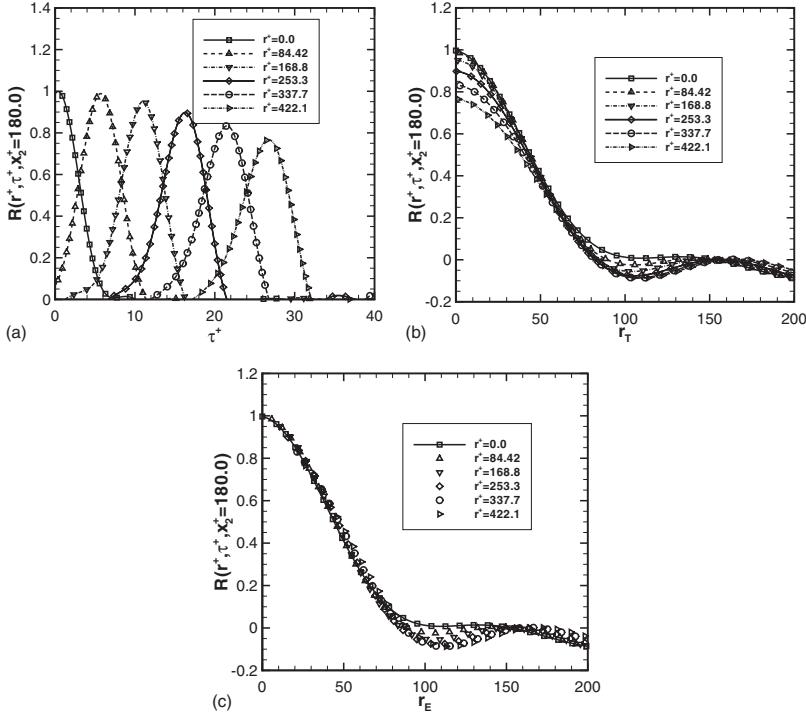FIG. 9. The space-time correlations R at $x_2^+ = 180.0$ for different space separations are plotted against (a) time separation, (b) the separation $r_T = r - Ut$ defined from Taylor's frozen flow hypothesis, and (c) the separation $r_E = \sqrt{(r-U\tau)^2 + (V\tau)^2}$ defined from the elliptic model, with parameters U and V obtained from curve fitting.

V. CONCLUSIONS AND DISCUSSIONS

The elliptic model suggests an interpretation of the decorrelation process of small eddies in turbulent shear flows. Small-scale eddies could change considerably by large-scale shear flows while they are carried past a given point by the mean flows and swept by the energy-containing eddies in fluctuation velocity fields. In the frozen flows, Taylor's model implies that the space-time correlation is solely determined by a convection velocity, which represents the dis-

placement of small eddies carried by large-scale eddies; in isotropic turbulence, the Kraichnan and Tennekes model suggests that the space-time correlation is mainly determined by a random sweeping velocity, which represents the distortions of smaller-scale eddies themselves. However, in turbulent shear flows, the large-scale flows induce the distortions of small eddies and thus accelerate the decorrelation process of small eddies. Therefore, in addition to convection and random sweeping velocities, the characteristic velocities for the
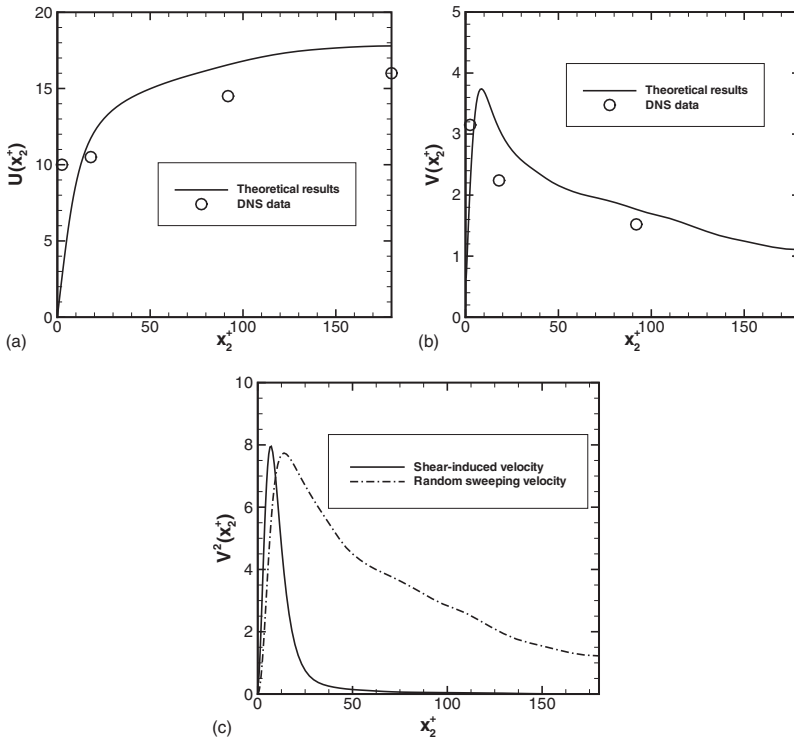

FIG. 10. The convection velocity and sweeping velocity: (a) convection velocity, (b) sweeping velocity, and (c) random sweeping velocity and shear-induced velocity.

space-time correlation in turbulent shear flows are compounded by the shear-induced velocity.

The elliptic model is supported by the DNS of turbulent channel flows. The space-time correlations for several fixed spatial separations are plotted against time separations and the normalized separations in terms of the elliptic model. The latter is found to collapse to a universal form as predicted by the elliptic model. In those plots, the convective and sweeping characteristic velocities are obtained by either direct calculations on the isocorrelation contours or curve fitting. Both of them yield satisfactory collapses. The elliptic model is based on the similarity assumptions on the isocorrelation contours. The data from DNS of turbulent channel flows justify that the contours have a uniform preference direction; the arguments from the Kolmogorov similarity hypotheses justify that the contours share a constant aspect ratio.

The elliptic model predicts a universal form for the space-time correlation in the inertial range at sufficiently high Reynolds numbers. It relates the space-time correlations to the space correlations via the convection and sweeping characteristic velocities. Therefore, the space-time correlations can be obtained from the form of space correlations (or energy spectra) and two characteristic velocities. Compare with the Taylor frozen flow hypothesis, the elliptic model can be used as an improved guideline to transform the temporal information from the one-point measurement with a single probe to the spatial one at different points. The accuracy of Taylor's frozen flow approximation depends on the flow properties such as a weak shear rate and lower turbulence intensity. The present model takes those two factors into account and is expected to better extract the energy spectra from experimental data. Meanwhile, this model has a useful implication to turbulence modeling. The recent applications of LES to aeroacoustics and turbulent mixing require the correct prediction of the space-time correlations. According to the elliptic model, this requires that the LES should correctly predict the space correlation and the convection velocity and the sweeping velocity. Noting that the sweeping velocity is determined by the properties of small-scale eddies such as the Taylor length microscales and the rms of for fluctuating velocities. These properties may not be recovered from the current subgrid-scale models. Therefore, the application of LES to this kind of problem raises new challenges to subgrid-scale modeling.

[1] R. H. Kraichnan, J. Fluid Mech. **5**, 497 (1959).

[2] D. C. Leslie, *Development in the Theory of Turbulence* (Oxford University Press, New York, 1973).

[3] C. Cambon and J. F. Scott, Annu. Rev. Fluid Mech. **31**, 1 (1999).

[4] E. Gkioulekas, Physica D **226**, 151 (2007).

[5] H. Chen, S. Chen, and R. H. Kraichnan, Phys. Rev. Lett. **63**, 2657 (1989).

[6] G.-W. He and Z.-F. Zhang, Phys. Rev. E **70**, 036309 (2004).

[7] J. Gleeson, Phys. Fluids **12**, 1472 (2000).

[8] Y. Zhou and R. Rubinstein, Phys. Fluids **8**, 647 (1996).

[9] M. Wang, J. B. Freund, and S. K. Lele, Annu. Rev. Fluid Mech. **38**, 483 (2006).

[10] G.-W. He, R. Rubinstein, and L. P. Wang, Phys. Fluids **14**, 2186 (2002).

[11] G.-W. He, M. Wang, and S. K. Lele, Phys. Fluids **16**, 3859 (2004).

[12] R. H. Kraichnan, Phys. Fluids **7**, 1723 (1964).

[13] H. Tennekes, J. Fluid Mech. **67**, 561 (1975).

[14] P. A. O'Gorman and D. I. Pullin, J. Turbul. **5**, 035 (2004).

[15] G. I. Taylor, Proc. R. Soc. London, Ser. A **164**, 476 (1938).

[16] C. C. Lin, Q. Appl. Math. **10**, 295 (1953).

[17] J. L. Lumley, Phys. Fluids **8**, 1056 (1965).

[18] L. S. G. Kovasznay, J. Aeronaut. Sci. **20**, 657 (1953).

[19] S. Corrsin, in Proceeding of the Oxford Symposium on Atmospheric Diffusion and Air Pollution (Academic, New York, 1960), p. 162.

[20] W. R. C. Phillips, Phys. Fluids **12**, 2056 (2000).

[21] G. W. He and J. B. Zhang, Phys. Rev. E **73**, 055303(R) (2006).

[22] R. H. Kraichnan, J. Fluid Mech. **41**, 189 (1970).

[23] T. Gotoh and Y. Kaneda, Phys. Fluids A **3**, 2426 (1991).

[24] A. Favre, J. Gaviglio, and R. Dumas, in *Mecanique de la Turbulence*, edited by A. J. Favre (CNRS, Paris, 1962), pp. 419–445.

[25] J. A. B. Wills, J. Fluid Mech. **20**, 417 (1964).

[26] G. T. Csanady, J. Atmos. Sci. **20**, 201 (1963).

[27] H. Choi and P. Moin, Phys. Fluids A **2**, 1450 (1990).

[28] A. S. Monin and A. M. Yaglom, *Statistical Fluid Mechanics*, edited by J. Lumley (MIT, Cambridge, MA, 1975), Vols. 1 and 2.

[29] J. O. Hinze, *Turbulence*, 2nd ed. (McGraw-Hill, New York, 1975).

[30] J. Kim and F. Hussain, Phys. Fluids A **5**, 695 (1993).

[31] M. Quadrio and P. Luchini, Phys. Fluids **15**, 2219 (2003).

[32] H. Tennekes and J. L. Lumley, *A First Course in Turbulence* (MIT, Cambridge, MA, 1999).

[33] Y. Kaneda and T. Gotoh, Phys. Fluids A **3**, 1924 (1991).

[34] X. Shen and Z. Warhaft, Phys. Fluids **12**, 2976 (2000).

[35] L. Biferale and F. Toschi, Phys. Rev. Lett. **86**, 4831 (2001).

[36] T. Ishihara, K. Yoshida, and Y. Kaneda, Phys. Rev. Lett. **88**, 154501 (2002).

[37] S. G. Saddoughi and S. V. Veeravalli, J. Fluid Mech. **268**, 333 (1994).

[38] T. Burghelea, E. Segre, and V. Steinberg, Phys. Fluids **17**, 103101 (2005).